ACS Macro Letters

Letter

pubs.acs.org/macroletters

10 nm Scale Cylinder–Cubic Phase Transition Induced by Caramelization in Sugar-Based Block Copolymers

Issei Otsuka,[†] Takuya Isono,[‡] Cyrille Rochas,[†] Sami Halila,[†] Sébastien Fort,[†] Toshifumi Satoh,[‡] Toyoji Kakuchi,*[,‡] and Redouane Borsali*[,†]

[†]Centre de Recherches sur les Macromolécules Végétales (CERMAV, UPR-CNRS 5301), affiliated with the Université Joseph Fourier (UJF) and member of the Institut de Chimie Moléculaire de Grenoble (ICMG, FR-CNRS 2607), BP53, 38041 Grenoble Cedex 9, France

[‡]Graduate School of Chemical Sciences and Engineering and Faculty of Engineering, Hokkaido University, Sapporo 060-8628, Japan

Supporting Information

ABSTRACT: To date, the feature size of microphase separation in block copolymers has been downsizing to 10 nm scale. However, morphological control for such a small feature is still a challenging task. The present Letter discusses a phase transition in a natural/synthetic "hybrid" block copolymer system based on an oligosaccharide and poly(ε-caprolactone) via thermal annealing. Time-resolved small-angle X-ray scattering investigation as a function of temperature indicated the phase transition from hexagonally close-packed cylinder to body-centered cubic at 10 nm scale. Atomic force microscope images of the block copolymer thin films annealed at different temperatures clearly confirmed the existence of these morphologies. The driving force of this phase transition (from cylinder to cubic) is the change of volume fraction of the block copolymer due to thermal caramelization.

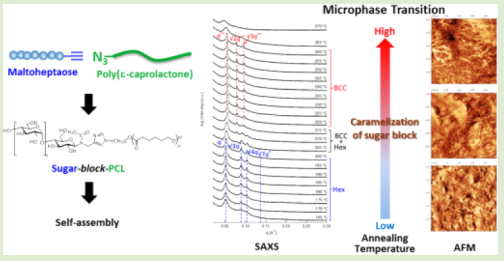

Microphase separation in block copolymers (BCPs) has been extensively studied and become one of the mainstreams of polymer science in nanotechnology over the past decade.[1,2] Recent advances in polymer synthesis such as controlled living polymerizations combined with "click" chemistry have enabled precise designs of BCPs having various block components with desired composition, molecular weight, and architecture. Thus, a growing interest is now focusing on designing devices for applications, such as solar cell, bit-pattern media, drug carrier, etc., via a so-called "bottom-up" approach using BCP self-assembly.[2,3] The main advantage of such an approach is that the feature size of the microphase structure can be reduced by decreasing the degree of polymerization (N) of BCP within the range of the product of N and the Flory–Huggins interaction parameter (χ); i.e., χN is larger than a critical value (10.5 for symmetric diblock BCPs).[1] Recently, several research groups reported microphase separation of BCPs with a much smaller feature than the limitation of the "top-down" approach (~20 nm).[4−7]

Poly- or oligosaccharide-based "hybrid" BCPs, which have high χ due to strong incompatibility between saccharidic and synthetic polymer blocks, are one of the promising candidates for the minimization of BCP microdomains. The hybrid BCPs consisting of polystyrene and malto-oligosaccharides were, indeed, phase separated into microdomains with ca. 10 nm feature size.[8] Such small microdomains were further functionalized by replacing the synthetic polymer block from standard polystyrene by a silicon-containing polystyrene derivative. The resulting microdomains have high reactive ion etching contrast between the natural saccharidic domain and the silicon-containing domain which is highly resistant to oxygen plasma.[9] Thus, it is becoming very important to broaden the class of the hybrid BCP system by coupling saccharidic blocks with functional polymers for potential applications in nanotechnology.

In this study, hybrid BCPs consisting of maltoheptaose (MH) and poly(ε-caprolactone) (PCL) were synthesized, and their self-assembly behaviors were investigated as a function of annealing temperature. PCL is a biodegradable polyester which has crystalline property. BCPs containing a crystalline block component have been widely studied due to their unique self-assembly behaviors dominated by crystallization combined with microphase separation.[2,3] The self-assembly of such BCPs is intricately intertwined with melting or crystalline temperatures (T_m or T_c) of the crystalline block and glass transition temperature (T_g) of the other block. When one of the block components is sugar, thermal caramelization,[10,11] i.e., decomposition and/or deformation of sugar, also affects the self-assembly. Herein, we demonstrate the effects of these thermal properties on the microphase transition of the hybrid BCP systems.

The azido end-functionalized PCL (**PCL-N_3**) was precisely synthesized by organocatalytic living ring-opening polymerization using an azido functionalized initiator (Scheme 1a). The

Received: October 15, 2012
Accepted: November 14, 2012
Published: November 19, 2012

Scheme 1. Strategy Used for the Synthesis of MH-*b*-PCL$_{(5k \text{ and } 10k)}$: (a) Synthesis of Azido End-Functionalized Poly(ε-caprolactone) and (b) "Click" Reaction between PCL-N$_3$ and Propargyl-MH

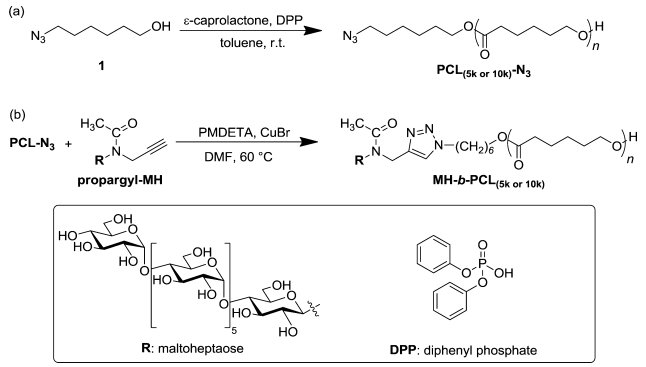

ring-opening polymerization of ε-caprolactone using diphenyl phosphate (DPP) as an organocatalyst proceeded in a living manner, and the molecular weight of the obtained polymer was well controlled with narrow polydispersities (Table 1). The

Table 1. Synthesis of PCL$_{5k}$-N$_3$ and PCL$_{10k}$-N$_3$[a]

sample	$M_{n,theo}$[b]	$M_{n,NMR}$[b]	$M_{n,SEC}$[c]	M_w/M_n[c]
PCL$_{5k}$-N$_3$	4650	4890	15200	1.04
PCL$_{10k}$-N$_3$	10200	10320	25100	1.07

[a]Polymerization condition: Ar atmosphere; solvent, toluene; temp., 27 °C. [b]Estimated by ^{1}H NMR. [c]Estimated by SEC in DMF containing 0.01 mol L^{-1} LiCl as PSt standard.

details of the polymerization have been reported elsewhere.[12] The **PCL$_{5k}$-N$_3$** and **PCL$_{10k}$-N$_3$** building blocks were coupled with propargyl-functionalized maltoheptaose (**propargyl-MH**) through copper-catalyzed azide−alkyne cycloaddition (CuAAC) in DMF as a good solvent for both **PCL-N$_3$** and **propargyl-MH**. Finally, diblock BCPs consisting of PCL and MH blocks (**MH-*b*-PCL$_{5k \text{ and } 10k}$**), characterized by ^{1}H NMR, IR, and SEC analyses (see Supporting Information), were obtained.

A small-angle X-ray scattering (SAXS) study was performed on the bulk BCP samples at different temperatures. The SAXS profiles of the BCP samples were measured in real-time using a synchrotron light source when increasing the temperature step-by-step. The SAXS profiles of **MH-*b*-PCL$_{5k}$** and **MH-*b*-PCL$_{10k}$** shown, respectively, in Figure 1a and 1b were drastically varied through the heating process. Broad SAXS profiles without any scattering peaks were observed in both **MH-*b*-PCL$_{5k}$** and **MH-*b*-PCL$_{10k}$** systems at 25 °C. Distinct primary scattering peaks (q^*) were then observed in both systems when heating above 65 °C. This result indicates that the mobility of BCP chains increased by heating the samples above T_m of the PCL blocks, which is clearly observed around 60 °C in the DSC profiles shown in Figure 2, demonstrating that the BCP systems self-organized into thermodynamically stable phases. Higher-order scattering peaks were observed by further enhancing the mobility of BCP chains through heating to achieve equilibrium phases; e.g., the peaks at $\sqrt{3}q^*$, $\sqrt{4}q^*$, and $\sqrt{7}q^*$ positions observed in the SAXS profile of **MH-*b*-PCL$_{5k}$** from 165 to 200 °C (Figure 1a) indicate a hexagonally close-packed cylinder phase (Hex), and the peaks at $\sqrt{2}q^*$, $\sqrt{3}q^*$, $\sqrt{4}q^*$, and $\sqrt{5}q^*$ positions observed for **MH-*b*-PCL$_{10k}$** from 135 to 250 °C

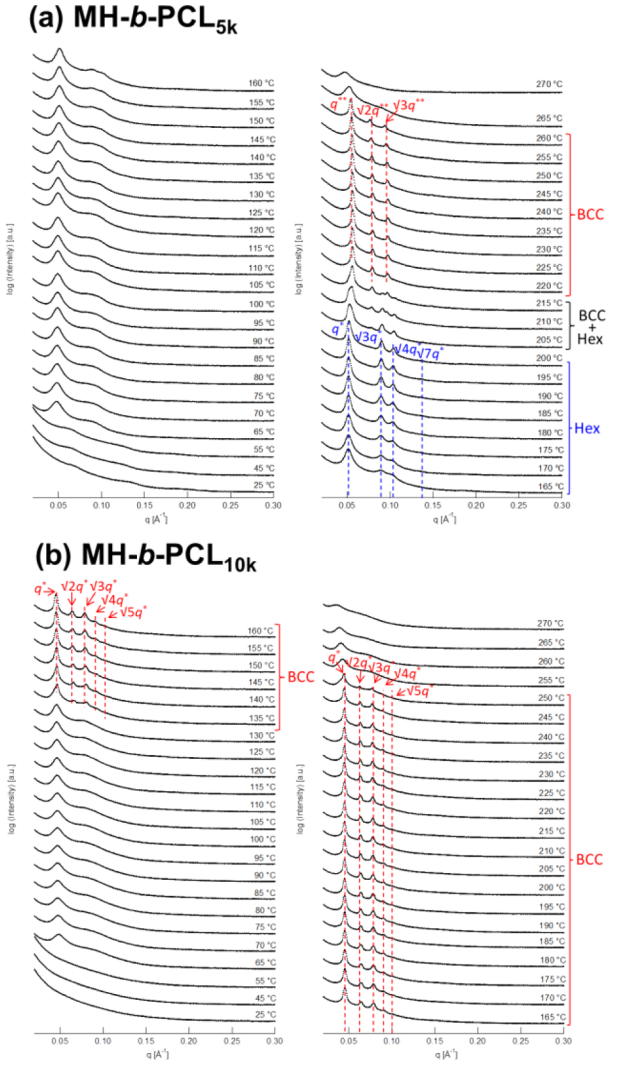

Figure 1. Variation of SAXS profiles of (a) **MH-*b*-PCL$_{5k}$** and (b) **MH-*b*-PCL$_{10k}$** during heating from 25 to 270 °C.

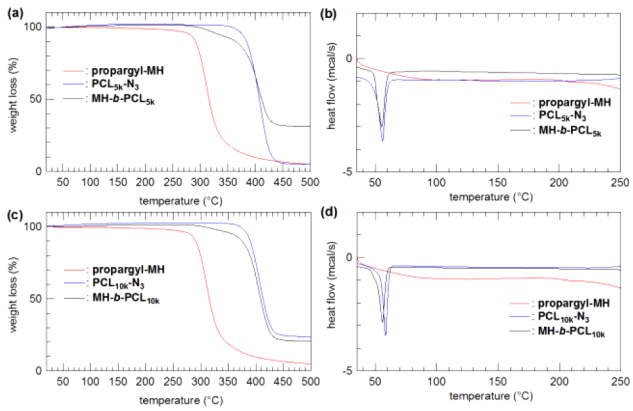

Figure 2. TGA and DSC profiles of **propargyl-MH**, **PCL$_{5k}$-N$_3$**, and **MH-*b*-PCL$_{5k}$** (a and b) and **propalgyl-MH**, **PCL$_{10k}$-N$_3$**, and **MH-*b*-PCL$_{5k}$** (c and d).

(Figure 1b) indicate a body-centered cubic phase (BCC). These equilibrium nano-organized phases were obtained by heating the BCP samples around the T_g of MH (T_g = 161 °C),[13] while distinct T_g values of the BCPs were not observed in the DSC profiles (Figure 2). At this temperature range, **MH-**

dx.doi.org/10.1021/mz300543u | *ACS Macro Lett.* 2012, 1, 1379−1382

b-PCL$_{5k}$ having a high volume fraction of the MH block (ϕ_{MH} = 0.18) is in the Hex phase of the phase diagram, and **MH-b-PCL$_{10k}$** having a low volume fraction of the MH block (ϕ_{MH} = 0.09) is in the BCC phase (Figure 3). Domain spacing (d) of

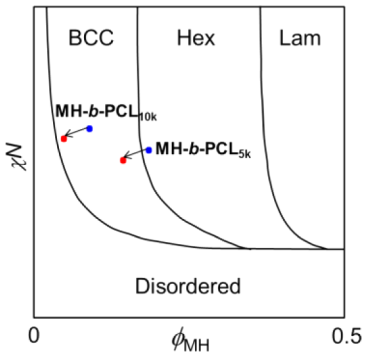

Figure 3. Schematic of the conceptual phase diagram of the **MH-b-PCL** system and the phases of **MH-b-PCL$_{5k}$** and **MH-b-PCL$_{10k}$** before (blue dot) and after (red dot) thermal caramelization.

these Hex and BCC morphologies was calculated to be 12.2 and 14.0 nm, respectively, by using Bragg's equation given below.

$$d = \frac{2\pi}{q^*}$$

Interestingly, a drastic phase transition was also observed when further heating **MH-b-PCL$_{5k}$**. Indeed, the SAXS profile of **MH-b-PCL$_{5k}$** was modified with a shift of q^* and higher-order scattering peaks by heating above 205 °C. In the temperature range from 220 to 260 °C, the SAXS profile of **MH-b-PCL$_{5k}$** showed distinct q^{**} and higher-order peaks at $\sqrt{2}q^{**}$ and $\sqrt{3}q^{**}$ positions, which corresponds to BCC morphology with d = 11.2 nm (Figure 1a).

This microphase transition from Hex to BCC was also supported by atomic force microscope (AFM) imaging. Figure 4 shows AFM phase images of **MH-b-PCL$_{5k}$** thin film samples, prepared by spin-coating BCP solution in THF onto silicon substrates and then heat annealing at different temperatures, and corresponding bulk SAXS profiles. Randomly oriented cylindrical morphology at 150 °C (Figure 4a) was aligned more parallel (mixture of horizontal and perpendicular orientation to the surface) at 190 °C with distinct sharpening of peaks in the SAXS profile (Figure 4b). Circular morphology corresponding to the BCC phase was observed in the AFM image of 240 °C with distinct peaks in the SAXS profile (Figure 4c). One notes here that the phase behavior of self-assembled diblock BCPs is dominated by the volume fraction of each block (ϕ), N, and χ in the phase diagram.[1] Thus, the phase transition occurs when one of these parameters is changed by external stimuli. In the present case, **MH-b-PCL$_{5k}$** (ϕ_{MH} = 0.18) should lie close to the phase boundary between Hex and BCC in the phase diagram, and the effective volume fraction of the MH block was slightly decreased because of the caramelization process[10,11] through heating to more than 200 °C. As a result, the phase of **MH-b-PCL$_{5k}$** moved from the HEX part to the BCC part in the phase diagram (Figure 3). Indeed, the TGA profile of **propargyl-MH** shows slight weight loss from ca. 200 °C before a significant decrease around 270 °C due to carbonization of the MH block (Figure 2). On the other hand, such a phenomenon was not observed for **MH-b-PCL$_{10k}$**; i.e., the SAXS profile of **MH-b-PCL$_{10k}$** was not changed at the temperature range from 135 to 250 °C (Figure 1b). Because of the low volume fraction of MH block in **MH-b-PCL$_{10k}$** (ϕ_{MH} = 0.09), **MH-b-PCL$_{10k}$** should be deeply embedded in the BCC part and further from the border to the Hex part in the phase diagram (Figure 3). Thus, the slight decrease of the effective volume fraction of MH due to caramelization did not affect the morphology of **MH-b-PCL$_{10k}$** in this temperature range. Finally, order−disorder phase transitions were observed in the SAXS profiles of both **MH-b-PCL$_{5k}$** and **MH-b-PCL$_{10k}$** by heating to 270 °C due to the carbonization of the MH block which is clearly observed in the TGA profile of **propargyl-MH** (Figure 2).

In summary, the hybrid BCPs consisting of MH and PCL self-organized into 10 nm scale cylinder or cubic microphases depending on the volume fraction and thermal annealing temperature. In the temperature range above T_m values of the PCL blocks and around the T_g of the MH block, **MH-b-PCL$_{5k}$**

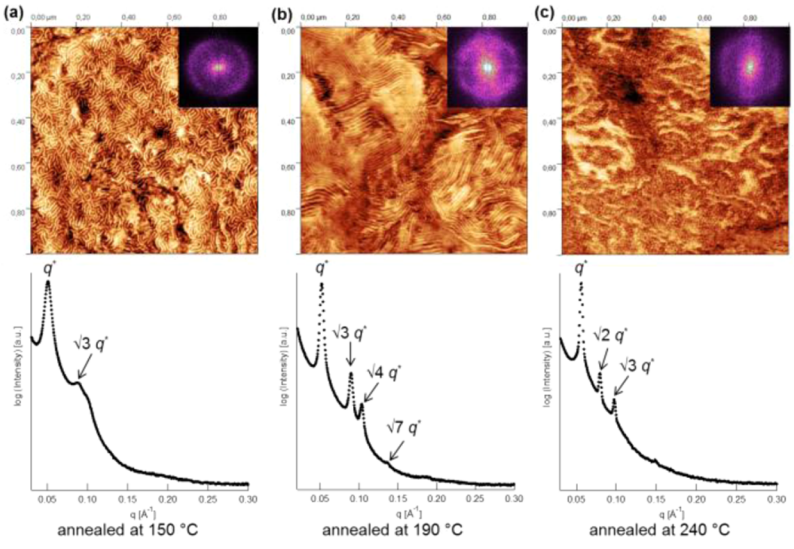

Figure 4. AFM thin film phase images with their 2D Fourier-transformed images (upper) and bulk SAXS profiles (lower) of **MH-b-PCL$_{5k}$** annealed for 30 min at (a) 150 °C, (b) 190 °C, and (c) 240 °C.

dx.doi.org/10.1021/mz300543u | ACS Macro Lett. 2012, 1, 1379−1382

and **MH-*b*-PCL$_{10k}$** self-organized into Hex and BCC phases, respectively. The thermal caramelization of the MH block above ca. 200 °C caused a decrease in ϕ_{MH}, leading to microphase transition of **MH-*b*-PCL$_{5k}$**, which lies near the boundary between Hex and BCC phases in the phase diagram. Such a microphase transition induced by caramelization is a step further toward morphological control for sugar-based BCPs.

EXPERIMENTAL SECTION

Film Preparation. BCP thin films were prepared for AFM observation by spin coating 0.5% (w/w) polymer solutions in THF at 2000 rpm for 30 s onto a silicon (100) wafer with a native oxide surface. These thin film samples were annealed under vacuum at different temperatures during 30 min and then put out to the air for quenching.

Small-Angle X-ray Scattering (SAXS) Measurements. SAXS experiments were performed on the BM02 beamline of the European Synchrotron Radiation Facility (ESRF, Grenoble, France). Bulk samples were put into glass capillaries of 1.5 mm diameter and then flame-sealed. These samples were disposed in sample holders equipped with an integrated heating system. The experiments were performed using 15 keV X-rays during heating in step-by-step. The sample temperature was controlled as follows: The samples were heated stepwise by 5 °C and kept at that temperature for 5−25 s (depending on the temperature) before measurement. Scattered intensities were recorded during 2−5 s exposures on a CCD detector (Ropper Scientific) placed about 80 cm behind the sample. The scattering intensities were corrected for grid distortion, the detector response, dark current, and sample transmission. A silver behenate sample was used for calibrating the q scale.

AFM Observations. AFM phase images were realized by tapping mode using a silicon cantilever (VISTA probes, Nanoscience Instruments, Inc., AZ, USA) with a tip radius of <10 nm, a resonant frequency of 190 kHz, and a force constant of 48 N/m.

ASSOCIATED CONTENT

Supporting Information

Information includes the synthesis and characterization of polymers. This material is available free of charge via the Internet at http://pubs.acs.org.

AUTHOR INFORMATION

Corresponding Author

*E-mail: borsali@cermav.cnrs.fr (R.B.); kakuchi@poly-bm.eng.hokudai.ac.jp (T.K.).

Notes

The authors declare no competing financial interest.

ACKNOWLEDGMENTS

R.B. acknowledges financial support from the Nanosciences foundation RTRA project "Hybrid Copolymer Systems" RTRA (Grant No. FCSN-2007-13P). This work was also supported by a Grant-in-Aid for Japan Society for the Promotion of Science (JSPS) Fellows to T.I. and the MEXT (Japan) program "Strategic Molecular and Materials Chemistry through Innovative Coupling Reactions" of Hokkaido University. The authors thank Ms. P. Chaud, Ms. S. Ortega Murillo, and Dr. C. Travelet for their help in the synthesis and characterization of polymers. Dr. F. Dubreuil is acknowledged for his help in the AFM observations. French collaborative group D2AM at ESRF is also acknowledged for beam time allocation. The authors thank Hayashibara Biochemical Laboratories for providing Maltoheptaose.

REFERENCES

(1) Bates, F. S.; Fredrickson, G. H. *Phys. Today* **1999**, *52*, 32−38.
(2) Kim, J. K.; Yang, S. Y.; Lee, Y.; Kim, Y. *Prog. Polym. Sci.* **2010**, *35*, 1325−1349.
(3) Kim, H.-C.; Park, S.-M.; Hinsberg, W. D. *Chem. Rev.* **2010**, *110*, 146−177.
(4) Son, J. G.; Hannon, A. F.; Gotrik, K. W.; Alexander-Katz, A.; Ross, C. A. *Adv. Mater.* **2011**, *23*, 634−639.
(5) Jung, Y. S.; Chang, J. B.; Verploegen, E.; Berggren, K. K.; Ross, C. A. *Nano Lett.* **2010**, *10*, 1000−1005.
(6) Park, S.; Lee, D. H.; Xu, J.; Kim, B.; Hong, S. W.; Jeong, U.; Xu, T.; Russell, T. P. *Science* **2009**, *323*, 1030−1033.
(7) Hirai, T.; Leolukman, M.; Liu, C. C.; Han, E.; Kim, Y. J.; Ishida, Y.; Hayakawa, T.; Kakimoto, M.; Nealey, P. F.; Gopalan, P. *Adv. Mater.* **2009**, *21*, 4334−4338.
(8) Aissou, K.; Otsuka, I.; Rochas, C.; Fort, S.; Halila, S.; Borsali, R. *Langmuir* **2011**, *27*, 4098−4103.
(9) Cushen, J. D.; Otsuka, I.; Bates, C. M.; Halila, S.; Fort, S.; Rochas, C.; Easley, J. A.; Rausch, E. L.; Thio, A.; Borsali, R.; Willson, C. G.; Ellison, C. J. *ACS Nano* **2012**, *6*, 3424−3433.
(10) Kroh, L. W.; Jalyschko, W.; Hgseler, J. *Starch* **1996**, *48*, 426−433.
(11) Kroh, L. W *Food Chem.* **1994**, *51*, 373−379.
(12) Makiguchi, K.; Satoh, T.; Kakuchi, T. *Macromolecules* **2011**, *44*, 1999−2005.
(13) Imamura, K.; Sakaura, K.; Ohyama, K.; Fukushima, A.; Imanaka, H.; Sakiyama, T.; Nakanishi, K. *J. Phys. Chem. B* **2006**, *110*, 15094−15099.